Journal of Geophysical Research: Atmospheres

RESEARCH ARTICLE
10.1029/2018JD028286

Convective Hydration of the Upper Troposphere and Lower Stratosphere

Mark R. Schoeberl[1], Eric J. Jensen[2], Leonhard Pfister[2], Rei Ueyama[2], Melody Avery[3], and Andrew E. Dessler[4]

[1]Science and Technology Corporation, Columbia, MD, USA, [2]NASA Ames Research Center, Moffett Field, CA, USA, [3]NASA Langley Research Center, Hampton, VA, USA, [4]Department of Meteorology, Texas A&M University, College Station, TX, USA

Key Points:
- Tropical convection increases stratospheric water vapor, but by less than 2%
- Only convection that penetrates the tropical tropopause significantly impacts stratospheric water
- Tropical convection is a major source of upper tropospheric clouds

Correspondence to:
M. R. Schoeberl,
mark.schoeberl@mac.com

Citation:
Schoeberl, M. R., Jensen, E. J., Pfister, L., Ueyama, R., Avery, M., & Dessler, A. E. (2018). Convective hydration of the upper troposphere and lower stratosphere. *Journal of Geophysical Research: Atmospheres*, *123*, 4583–4593. https://doi.org/10.1029/2018JD028286

Received 5 JAN 2018
Accepted 9 APR 2018
Accepted article online 18 APR 2018
Published online 6 MAY 2018

Abstract We use our forward domain filling trajectory model to explore the impact of tropical convection on stratospheric water vapor (H_2O) and tropical tropopause layer cloud fraction (TTLCF). Our model results are compared to winter 2008/2009 TTLCF derived from Cloud-Aerosol Lidar with Orthogonal Polarization and lower stratospheric H_2O observations from the Microwave Limb Sounder. Convection alters the in situ water vapor by driving the air toward ice saturation relative humidity. If the air is subsaturated, then convection hydrates the air through the evaporation of ice, but if the air is supersaturated, then convective ice crystals grow and precipitate, dehydrating the air. On average, there are a large number of both hydrating and dehydrating convective events in the upper troposphere, but hydrating events exceed dehydrating events. Explicitly adding convection produces a less than 2% increase in global stratospheric water vapor during the period analyzed here. Tropical tropopause temperature is the primary control of stratospheric water vapor, and unless convection extends above the tropopause, it has little direct impact. Less than 1% of the model parcels encounter convection above the analyzed cold-point tropopause. Convection, on the other hand, has a large impact on TTLCF. The model TTLCF doubles when convection is included, and this sensitivity has implications for the future climate-related changes, given that tropical convective frequency and convective altitudes may change.

Plain Language Summary Deep convection has been invoked as a significant source for stratospheric water vapor based on aircraft observations. This modelling study shows that deep convection plays almost no role in directly hydrating the stratosphere because deep convection rarely penetrates the tropopause 'cold trap' that largely controls stratospheric water vapor.

1. Introduction

The average global concentration of stratospheric water vapor (H_2O) is primarily determined by the transport and dehydration of air moving into the stratosphere through the tropical tropopause cold trap where ice forms and falls out. Water can also form through the oxidation of methane in the upper stratosphere. These processes have been known for nearly 70 years (Brewer, 1949; Fueglistaler et al., 2009; Randel & Jensen, 2013, and references therein).

Schoeberl et al. (2016) (S16) evaluated a number of processes that control the stratospheric water vapor and tropical tropopause layer cloud fraction (TTLCF). These processes include the tropopause temperature in the Modern-Era Retrospective analysis for Research and Applications (MERRA) versus MERRA-2, the ice nucleation relative humidity (RH), and high-frequency gravity waves that are typically absent in the reanalyses. We found that MERRA-2 with its colder tropopause than MERRA created a drier stratosphere unless the nucleation RH (NRH) was set higher than 100%. This result is consistent with aircraft observations (Jensen et al., 2013, 2016; Krämer et al., 2009) that show RH values as high as 160% in the tropical upper troposphere. We also found that high-frequency gravity waves could significantly increase the TTLCF while slightly increasing stratospheric water. This occurs because high-frequency gravity waves make the dehydration process less efficient by creating small ice crystals that settle more slowly than would occur without the waves (Schoeberl et al., 2015).

A fourth process is the injection of water into the stratosphere by strong convection. Both convection and diabatic upwelling supply water vapor to the upper tropical troposphere and play a role in determining the altitude of the tropopause (Randel & Wu, 2005; Son & Lee, 2007; Thuburn & Craig, 2002; Zhou & Holton, 2002). Midlatitude aircraft measurements suggest that overshooting convection can also move

water directly into the stratosphere bypassing dehydration by the cold trap (Anderson et al., 2012; Danielsen, 1993; Hanisco et al., 2007; Herman et al., 2017; Smith et al., 2017). Recent tropical aircraft measurements show tropical convective overshoots reaching into the lower stratosphere (Corti et al., 2008; Khaykin et al., 2009). Satellite measurements have also identified water vapor plumes in the lower midlatitude stratosphere associated with deep convection (Schwartz et al., 2013; Sun & Huang, 2015). More recently, Avery et al. (2017) showed observations of tropical convection penetrating 2 km above the interpolated MERRA-2 cold point tropopause during the 2015–2016 El Niño event.

The idea that convection can bypass the tropopause cold trap and directly inject water vapor and other trace gases into the lower stratosphere has been reinforced by observations of the unexpectedly large stratospheric concentration of the water isotopologue HDO. The ratio HDO/H_2O is a tracer of the parcel's convective history (Keith, 2000; Moyer et al., 1996; Pollock et al., 1980), and higher values of the HDO/H_2O ratio suggest convective sources of water. Sayres et al. (2010) analyzed the results from aircraft missions over Costa Rica and showed that convection appeared to be increasing both the HDO and H_2O amounts in the lower stratosphere. Most recently, Randel et al. (2012) analyzed the global HDO observations from the Atmospheric Chemistry Experiment Fourier transform spectrometer and found enhanced lower stratospheric HDO/H_2O ratios in the vicinity of convection over the North American monsoon, consistent with the idea that direct convective injection is a major source of stratospheric water. On the other hand, there was little enhancement over the Asian Monsoon. Randel et al. (2012) hypothesized that this was due to evaporation of convective ice in the subsaturated North American Monsoon lower stratosphere, whereas the lower stratosphere is saturated over the Asian Monsoon, and HDO-rich ice would fall out without evaporating. As these observations show, the link between convective sources of water and enhancements in HDO is not direct. For example, Dessler et al. (2007) showed that addition of water from evaporating convective ice in the tropical upper troposphere could explain the observed HDO concentration with little change in stratospheric water vapor. In other words, the stratospheric HDO abundance is much more sensitive to tropical convective processes than is H_2O (Sherwood & Risi, 2012).

From in situ observations of convective water vapor plumes and from HDO measurements, it would appear that convective transport of water into the lower stratosphere is occurring, but quantifying the global impact is difficult. The preliminary Lagrangian model study by Schoeberl et al. (2014) (S14) using MERRA reanalysis estimated that parameterized convection increases global stratospheric water by ~8%. Ueyama et al. (2015) estimated that convection increases the tropical upper troposphere water vapor concentration by 0.34 ppmv (14%) at ~100 hPa, which is just below the mean tropical tropopause. Ye et al. (2017) demonstrated that interannual variability in convection, mainly due to El Niño–Southern Oscillation, makes a small contribution to interannual variability in TTL water vapor at 100 hPa.

It is worth exploring the convective processes further to understand how future changes in convection might alter the water vapor amounts in the stratosphere (Dessler et al., 2016), alter cloudiness in the tropical upper troposphere, or impact lower stratospheric chemistry (Anderson et al., 2017). We focus on the Northern Hemisphere winter period since most of the diabatic transport of air into the stratosphere occurs during this period (e.g., Schoeberl & Dessler, 2011). This paper provides a more extensive analysis of the role of convection than reported in S14 and Ueyama et al. (2015). Here we use two different representations of tropical deep convection to quantify the impact of convection and explore the issue of tropical convective hydration versus dehydration. The central question addressed in this paper is as follows: How does convection impact the stratospheric water vapor and the TTLCF?

2. Model

2.1. Basic Model Description

The model used in this study is the forward domain filling trajectory model of Schoeberl and Dessler (2011) with the basic model configuration as described in S14 and S16 excepted as noted below. The forward domain filling model uses the Bowman and Carrie (2002) diabatic trajectory code with MERRA-2 winds, temperatures, and diabatic heating rates (Gelaro et al., 2017; Molod et al., 2015). Between ±45° latitude, 1,240 parcels are initiated at random locations each day along the 360 K potential temperature surface. Above that surface, which is usually just above the average zero diabatic heating line, parcels ascend into the upper troposphere/lower stratosphere (UTLS). Model parcels are removed when they fall below the

250-hPa surface—which occurs mostly at midlatitudes. Each parcel is started with a 95% RH with respect to ice (RH); the initial RH value does not affect our results. Methane oxidation is included as a source for water as described in Schoeberl and Dessler (2011). For all of our experiments, integration is started in the year 2000; the model takes about 2 years for the domain to fill. When the parcel RH exceeds the prescribed NRH, ice crystals are produced as part of our cloud model. The number of crystals generated is proportional to the parcel cooling rate (Kårcher et al., 2006). The crystals grow, depleting vapor, and gravitationally settle out of the parcel, dehydrating the air. Ice crystals can also evaporate as the parcel warms. The cloud parameterization is described in detail in S14 and S16.

Schoeberl et al. (2016) compared model results to Microwave Limb Sounder (MLS) and Cloud-Aerosol Lidar with Orthogonal Polarization (CALIOP) TTLCF. For NRH values between 130 and 150%, the model shows good agreement with observations. As in S16, we analyze the winter of 2008/2009; other winters show similar results (as indicated below). For comparisons with MLS we grid the trajectory water vapor fields and use the MLS averaging kernels.

2.2. Gravity Waves

High-frequency gravity waves, those with periods shorter than a day, are not included in the reanalysis fields. These gravity waves are assumed to have a temperature power spectrum of the form

$$T'^2 = T_o^2 (\omega / \omega_o)^{\alpha} \quad (1)$$

where α is the spectral dependence, ω is the frequency, ω_o is the daily frequency, and T_o is the temperature amplitude at the daily frequency. Schoeberl et al. (2015) and S16 discussed the impact of varying the high-frequency gravity wave temperature amplitudes on the model. As noted above, S16 found that gravity waves have a large effect on TTLCF and a small effect on water, but both increase as the wave amplitude increases. In order to link our results to S16, we start with model runs using altitude-independent low-amplitude gravity waves. In the absence of gravity wave information, the amplitude of these waves was tuned toward observed water vapor and the TTLCF.

Since S16, Schoeberl et al. (2017) analyzed 3 years of pressure perturbations recorded by Project Loon's lower stratospheric superpressure balloons. From 18 to 20 km the Loon wave amplitudes are ~0.7 K, more than twice as large as those used in S16. These larger wave amplitudes are consistent with other balloon observations of the lower stratosphere (Podglajen et al., 2016). Wave amplitudes of this magnitude, if assumed constant over the depth of the upper troposphere, produce an unrealistically large TTLCF. In order to create a more reasonable gravity wave amplitude profile, we use Kim and Alexander (2013) analysis of the vertical structure of tropical waves, attenuating the waves below the tropopause to less than half their tropopause amplitude (i.e., T_o at 15 km is 0.35 K).

2.3. Convection

2.3.1. Convection Data Sets

To estimate convective impact, we use both the MERRA anvil ice fields as well as a convection scheme based on satellite observations (SC), as in Ueyama et al. (2015). Anvil ice is an estimate of ice detraining from simulated convection and is available in the MERRA data distribution, but not in the MERRA-2 distribution. The same convective scheme, relaxed Arakawa-Schubert (RAS; Moorthi & Suarez, 1992), is used in both MERRA and MERRA-2. RAS is a statistical scheme used to simulate subgrid scale convection. Molod et al. (2015) discuss the implementation of RAS in the atmospheric general circulation model used in MERRA-2 and the differences between the MERRA and MERRA-2 implementation of RAS. Comparisons between the MERRA and MERRA-2 schemes show similar maximum heights for convection. We therefore assume that the MERRA anvil ice product provides a good estimate of the MERRA-2 anvil ice even with improved MERRA-2 dynamics. MERRA anvil ice fields are available once per day.

While using MERRA convection is likely not optimal, we use it for three reasons. First, MERRA convection was used in S16 so this allows us to compare the results shown in that paper. Second, MERRA convective tops are lower than SC, as shown below, so using MERRA allows us to show the impact of systematically lower convective heights. Third, RAS is used in GEOS5 and other atmospheric general circulation models, so the use of MERRA convection allows our results to apply to those models as well.

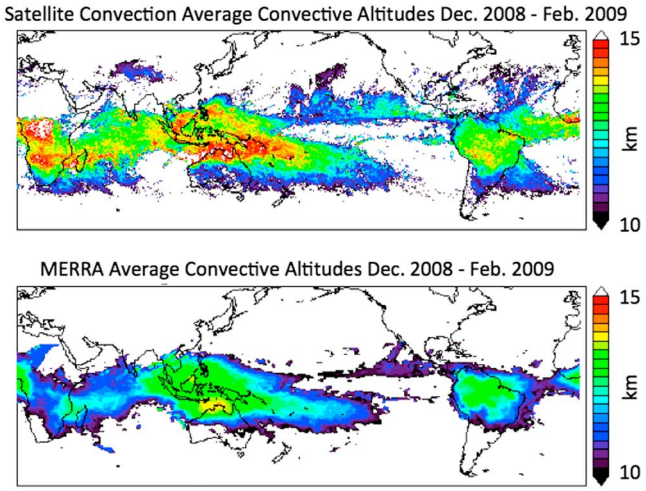

Figure 1. Comparison of (top) satellite based average convective altitudes and (bottom) Modern-Era Retrospective analysis for Research and Applications convective altitudes using anvil ice for DJF 2008/9. Both panels only include events above 10 km.

The SC scheme generates tropical convective cloud top pressure altitudes and potential temperatures using 3-hourly satellite global rainfall estimates and geostationary satellite brightness temperature data along with TRMM 3-hourly precipitation data to distinguish convective and in situ clouds (Bergman et al., 2012; Ueyama et al., 2014). The scheme reproduces the horizontal and vertical distributions of convective cloud top altitudes derived from the CloudSat deep convective cloud classification product as modified by concurrent CALIOP measurements. The SC product is available from 2006 to 2016 on a 0.25° grid from ±60°. Note that the SC grid is much finer than MERRA's 1.25° anvil ice grid and the SC height is not restricted to MERRA grid levels. We use the SC cloud top potential temperatures derived by matching the cloud top brightness temperatures to co-located reanalysis temperature profiles; the cloud top potential temperatures have an estimated uncertainty of ±5 K.

Figure 1 compares average convective heights for MERRA and SC over the 2008/2009 winter period. Both data sets show about the same geographic distribution, but SC covers a wider area and reaches higher altitudes than MERRA. Figure 2 shows the normalized frequency distribution of convective altitudes. The SC height decreases rapidly above 14 km, whereas MERRA convective heights decrease rapidly just above 13 km. These differences mean that more upper tropospheric parcels will be affected by convection when using SC in the model than when using MERRA.

2.3.2. Parcel Convective Interaction

When a trajectory parcel crosses a grid box identified as having convection, and the parcel is below the local peak convective altitude, ice is added to the parcel, and the RH is set to 100% as would occur inside a cloud. Convection does not supersaturate parcels. If the air is subsaturated before encountering convection, the parcel is hydrated. If the air is supersaturated before encountering convection, the parcel is dehydrated to 100% RH. The amount of convective ice added to the parcel, and the mean particle size and number are taken from the tropical convection observations of Frey et al. (2014, their Table 1). At the highest level potential temperatures (370–375 K) the convective ice effective radius is 6 μm with a number density of 10/L; at the lowest level potential temperatures (360–365 K) we use 15-μm radius with a number density of 450/L. Because the convective cloud is a saturated environment, added ice crystals fall out. Thus, even though we process the air with convective ice added to the cloud model, we find that adding ice makes a negligible change to TTL water vapor.

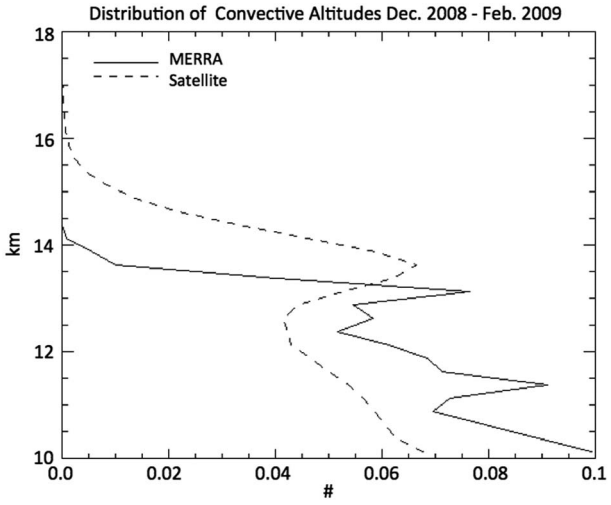

Figure 2. Normalized (to 1) distribution of satellite based average convective altitudes (dash) and Modern-Era Retrospective analysis for Research and Applications convective altitudes (solid) using anvil ice for DJF 2008/9. See Figure 1.

The trajectory model tracks the change in water vapor upon encountering convection, so we can tell whether convection hydrates or dehydrates the air parcel. In order to further determine the sensitivity of the model to uncertainties in estimated convective heights, we also perform experiments where we add 5 and 10 K to the satellite convection potential temperature altitude, making no other model changes.

3. Model Experiments and Results

In S16, we performed a series of experiments varying the NRH and gravity wave forcing to determine the response of the TTLCF and water vapor. S16 showed that increasing NRH creates a wetter stratosphere. Optimal global NRH values for best agreement with observed global stratospheric water vapor and TTLCF are likely between 160%, the homogeneous nucleation threshold at tropical tropopause temperatures, and 120%, roughly the heterogeneous nucleation threshold (Jensen et al., 2016). Thus, we choose these two values, 120% and 160%, to bracket our simulations.

Table 1
Summary of Convection Experiments, Results for Winter 2008/2009

Experiment	NRH	% Strat. parcels infl. by conv.	Dehydration/hydration	Strat. water (ppm), % diff. from no convection	TTLCF
% Diff from no convection					
1 No conv. + cg	160	N/A	N/A	4.65, -	0.11, -
2 MERRA + gg	160	3.8%	0.72	4.66, 0.2%	0.13, 18%
3 SC + cg	160	28%	0.75	4.68, 0.6%	0.26, 136%
4 SC + cg + 5 K	160	23%	0.57	4.69, 0.8%	0.34, 194%
5 SC + cg + 10 K	160	67%	0.62	4.81, 3.4%	0.59, 436%
6 No conv. + L	160	N/A	N/A	4.77, -	0.14, -
7 MERRA + L	160	3.8%	0.76	4.78, 0.2%	0.17, 21%
8 SC + L	160	24%	0.67	4.71, −1.2%	0.27, 92%
9 No conv. + L	120	N/A	N/A	4.47, -	0.22, -
10 MERRA + L	120	3.6%	0.63	4.47, 0%	0.23, 4.5%
11 SC + L	120	32%	0.75	4.53, 1.3%	0.34, 54%
MLS/CALIOP	-	-	-	4.59 ± 0.28	0.24 ± 0.024

Note. cg indicates constant altitude gravity waves with T_o set to 0.15 K. L indicates height varying gravity wave amplitudes based on Loon data as discussed in the text. +10 K means that 10 K is added to the convective height potential temperature. Water amount is the global average from 18–30 km as in S16. TTLCF is integrated cloud amount 16–18 km between ±20° latitude, a narrower range than that used in S16. Percentages in the last two columns indicate changes from the equivalent no convection case. For MLS we use V4.23; for CALIOP we use V4.1. The MLS H_2O uncertainty is ~6% (Livesey et al., 2017); for CALIOP TTLCF the estimated upper limit uncertainty is about 10%.

Schoeberl et al. (2016) used constant-altitude high-frequency gravity wave temperature perturbations (T_o) ranging between 0 and 0.35 K. Here we use 0.15 K. We also use the Loon gravity wave-altitude-varying T_o values described above. For both gravity wave schemes, α is set to −2 (equation (1); see section 2.2) as has been observed by both aircraft and balloon measurements (Bacmeister et al., 1996; Hertzog & Vial, 2001; Podglajen et al., 2016; Schoeberl et al., 2017).

As in S16, the results will be compared to TTLCF observations by CALIOP and water observations by MLS. All experimental results are summarized in Table 1 and Figure 3. Water vapor listed in the table is the global average water vapor from 18 to 30 km. Model TTLCF is computed as the number of cloudy parcels between 16 and 18 km and ±20° latitude divided by the total number of parcels in the same domain. CALIOP fractional area TTLCF is computed as total number of profiles with at least one cloudy pixel in 60-m vertical bins between 16 and 18 km, divided by the total number of observed profiles. The CALIOP data in S16 were V3, and now we use V4. Table 2 shows Exp. 8 (Table 1) stratospheric water vapor and TTLCF for the winters 2008–2013. As is evident from Table 2, there is little interannual variability in stratospheric water or in TCF, so our analysis of 2008/2009 should be broadly applicable.

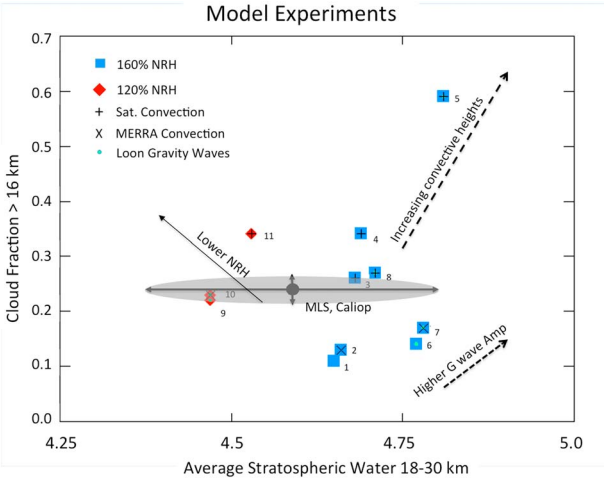

Figure 3. A summary of all the experiments listed in Table 1 as in S16. The colored symbols indicate the nucleation relative humidity (NRH) values used, with + and X to indicate the type of convection used. Experiments incorporating Loon gravity waves have embedded small green circles. The arrows indicate the tendency for each of the processes as investigated in this paper; changing NRH, convective height, and gravity waves.

As noted above, when air parcels encounter convection, we tag the parcel and record the change in water vapor produced by the encounter. Convection can increase or decrease water, and the dehydration/hydration ratio for all parcels that encounter convection is shown in Table 1. We also count the total number of stratospheric parcels (those above the tropopause) that have encountered convection above 360 K (the initialization level)—the percent of stratospheric parcels influenced by tropospheric convection is the convective influenced parcels divided by the total number of stratospheric.

3.1. The Impact of High-Frequency Gravity Waves and Changing NRH on TTLCF and Water in the Absence of Convection

We first address the impact of gravity waves, since the Loon gravity wave parameterization is quite different from the constant altitude parameterization used in S16 and previous studies such as Jensen and Pfister (2004). As mentioned in the introduction, we showed in S16 that the addition of high-frequency gravity waves increased

Table 2
Stratospheric Water and TTLCF[a]

Year (DJF)	Strat. water (ppm)	TTLCF
2008	4.71	0.27
2009	4.74	0.26
2010	4.78	0.26
2011	4.78	0.25
2012	4.82	0.26
2013	4.82	0.26

[a]See Table 1, Exp. 8.

TTLCF and, to a lesser extent, stratospheric water. The relative increase in stratospheric water occurs because the high-frequency temperature oscillations reduce dehydration efficiency (Schoeberl et al., 2015).

Comparing Exp. 1 (no convection, 0.15 K constant gravity wave) results and Exp. 6 (no convection, higher amplitude Loon-based gravity waves), we see the same effect. The higher wave amplitude Loon scheme has ~2% more stratospheric water and ~27% more cloud than the constant gravity wave scheme. Exp. 1 produces more stratospheric water than Exp. 9 (120% NRH, no convection) simulation as found by S16. Note that compared to MLS, all simulations are within the MLS uncertainty (Figure 3), but all three "no convection" simulations produce too little cloud.

3.2. Convection

3.2.1. Change in Stratospheric Water and TTLCF Due to Convection

In S14, which used MERRA reanalysis, we reported that adding MERRA convection would increase stratospheric water between 8% and 6%, a much larger value than shown in Table 1. MERRA reanalysis has a much warmer tropopause than MERRA-2 (see S16), and thus, convective increases in upper tropical troposphere water will have a larger impact on the stratosphere. This expectation is consistent with the changes in water vapor shown in Table 1 with the altitude independent gravity wave experiments (Exp. 1–5) and with NRH at 160%.

In each of the successive experiments, Exp. 1–5, convective height increases. MERRA convection (Exp. 2) has the lowest heights (see Figure 2); SC + 10 K (Exp. 5) has the highest. When the convective heights increase between MERRA and SC, stratospheric water vapor increases as well, but only slightly. In our model, convection below the tropopause has little impact on stratospheric water vapor because tropopause temperature largely controls the stratospheric water vapor. The higher the convection penetrates above the tropopause, the larger the impact on stratospheric water (Dessler et al., 2007). This is clearly seen with Exp. 5 where the convection is extended into the stratosphere by adding 10 K to the height. In Exp. 5, stratospheric water vapor increases by more than 3% compared to no convection.

Increasing the convective height increases the probability of encountering convection. We calculate that about 2.9% of stratospheric parcels encounter convection in the stratosphere (above 380 K) for Exp. 4 versus 0.8% for Exp. 3. A 5 K increase in convective height (Exp. 4) is within the range of uncertainty of the SC cloud top height; however, the TTLCF now increases by ~200% which is greater than observed. With a 10 K increase in convective height, TTLCF increases enormously, 454%. The larger impact on cloudiness occurs because more convective systems extend into the upper troposphere, causing more saturated air. Diagnostic maps for both experiments (not shown) indicate that cirrus cover dramatically increases and, in the 10 K case, almost completely covers the tropics.

Experiments 6–8 show the results when we use the Loon gravity waves at 160% NRH. We have similar results with the fixed gravity wave experiments, a small increase in water vapor, but a dramatic increase in TTLCF. For the 160% NRH, SC, Loon case (Exp. 8), stratospheric water vapor actually decreases slightly compared to the "no convection" case. This result can be explained by the fact that convection brings parcels closer to 100% RH—effectively drying out the supersaturated environment before stratiform cloud nucleation can occur. This effect is only seen when the NRH is highest and gravity waves are large so that cloud dehydration is very inefficient (Schoeberl et al., 2015).

For the last series of experiments 9–11 we lower the NRH. The response is similar to the previous cases except the stratospheric water is about 0.2 ppmv lower and the cloud fraction about 0.1 higher. The decrease in water is due to the fact that parcels entering the stratosphere are drier than in the 160% NRH case and the dehydration of the parcels produces more cloud as well (S16). Exp. 11, Loon + SC is within the observed range for water, but TTLCF is higher than observed.

3.2.2. Domain of Winter Convective Influence

Figure 1 shows that the strongest winter convection is south of the equator for both SC and MERRA. Figure 4 shows the vertical location of convective influence events over the winter period comparing MERRA and SC

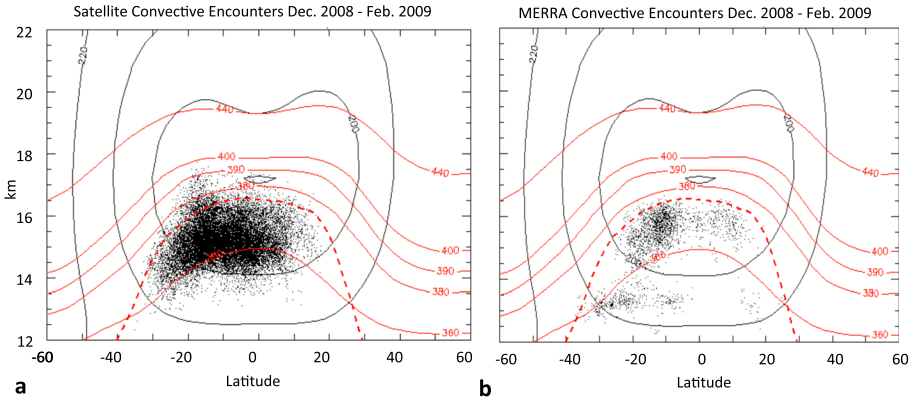

Figure 4. Location of convective influence events. (a) For convective system (Exp. 7) and (b) for Modern-Era Retrospective analysis for Research and Applications convection (Exp. 6). The dashed line is the zonal mean tropopause. The solid black lines are the zonal mean temperature, and the red lines are selected potential temperature surfaces as labeled.

(Exp. 7 and 8)—convective influence events are defined here as parcel locations where water vapor changes through an encounter with convection. Figure 4a shows that SC convection has a significantly larger number of convective influence events than MERRA convection (Figure 4b), as might be expected from Figures 1 and 2, and these events are mostly in the Southern Hemisphere during the Boreal winter season.

3.2.3. Hydration Versus Dehydration by Convection

For convective influence events, we record the ΔH_2O. From parcel initialization to arriving in the stratosphere, multiple convective encounters can occur. Even though we analyze only the last convective encounter, our statistics qualitatively represent the overall influence of convection in the upper tropical troposphere. Table 1 shows the percent of stratospheric parcels that have had convective encounters. We also show the ratio of dehydration to hydration events that have occurred for parcels during our winter period. For SC convection, ~25% of the parcels directly encounter convection after being initialized at 360 K before making it into the stratosphere. For MERRA convection, only ~4% of the parcels encounter convection.

When ΔH_2O is less than zero, we define the convective event as dehydration and vice versa for hydration. Table 1 shows that the ratio of dehydration to hydration events is ~0.7, meaning that both kinds of events occur but hydration events always exceed dehydration events. Dehydration events appear to be mixed in with hydration events as shown in Figure 5—both are occurring within the population of all convective events.

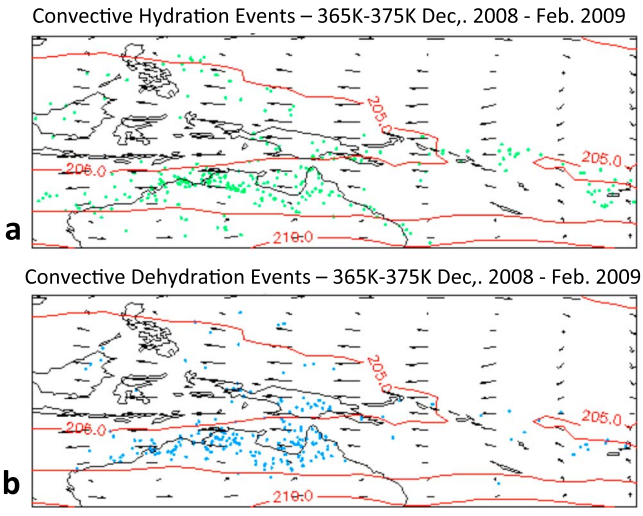

Figure 5. (a) Location of convective hydration events between 365 and 375 K; (b) location of convective dehydration events in the same region. The red contours show temperatures on the 365 K potential temperature surface. The arrows show the wind vectors on that surface.

Figure 6 shows the number of convective events reaching high potential temperatures during winter, and the vertical distribution of convective influence events over the 2008 winter period. The decrease in convective influence with altitude is consistent with the decrease in number of convective events reaching higher altitudes (Figure 2). These results are also consistent with the impact of convection on TTL cirrus noted by Ueyama et al. (2015).

4. Summary and Discussion

We have performed a series of model experiments to determine the impact of deep tropical convection on stratospheric water vapor and TTLCF. We vary high-frequency gravity wave amplitudes, the NRH, and we use two convection data sets—a reanalysis RAS-based convective data set and a satellite observation-based data set to assess convective impact. We focus on the 2008–2009 winter period; we show that results for this winter are typical (Table 2). Our experiments (summarized in Table 1 and Figure 3) show that is it fairly easy to reproduce the observed global averaged stratospheric water vapor content with a variety of NRH thresholds, gravity wave amplitudes,

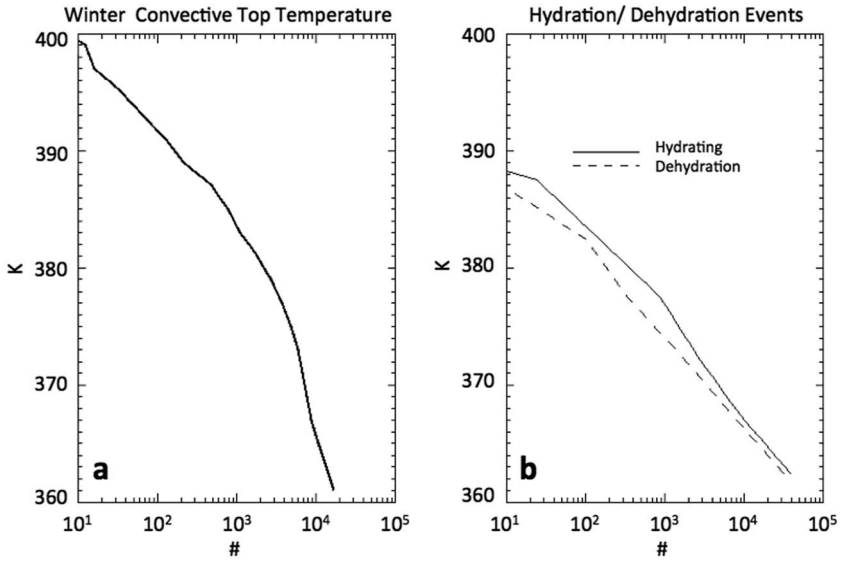

Figure 6. (a) Global number convective system events reaching the indicated potential temperature over the 2008 winter period showing the decrease in convective events reaching higher altitudes. (b) Vertical distribution of convective hydration (solid) and dehydration (dashed) events between ±30° latitude. Because there can be more than one convective encounter per convective event, the two distributions in (a) and (b) are not equivalent.

and either convection data sets. TTLCF is much more sensitive to our choice of parameterizations. Very large increases in cloud fraction can occur for larger gravity wave amplitudes and with increased convective altitudes.

4.1. Impact of Convection

High-altitude aircraft has observed localized convective hydration (Anderson et al., 2012; Corti et al., 2008; Danielsen, 1993; Hanisco et al., 2007; Herman et al., 2017; Khaykin et al., 2009; Kley et al., 1982; Smith et al., 2017); however, our calculations show that these events contribute $<$1% to the global stratospheric water vapor budget. Even if we narrow the range of impact to the tropical lower stratosphere (less than 30° latitude) the impact is 1–2%, much smaller than the 5–10% tropical increase computed by S14 using MERRA reanalysis. We attribute these differences to the warmer MERRA tropopause meteorological fields (see S16). Ueyama et al.'s (2015) estimate of a 7% increase in tropical water due to convection applies to a region below the tropical tropopause, a zone that will experience a larger convective impact, and a narrower domain. For the same domain, we estimate a 6.25% increase in water vapor, in close agreement with Ueyama et al. (2015).

Avery et al. (2017) analyzed the anomalous East Pacific convection during the 2015–2016 El Niño. Their results suggested that there was large regional water vapor impact due to this convection. CALIOP observations show that during this El Niño event, convective events extended up to 2 km above the tropopause (~60 K increase in potential temperature). This is far higher than previously seen in the 10-year CALIOP Central Pacific data record. The Avery et al. estimate of the contribution to tropical lower stratospheric water vapor by convection was ~0.3 ppm. When averaged over the global stratospheric domain for comparison with Table 1, this amount is ~0.1 ppm, about half the increase shown in Exp. 5, where all convective heights were increased by 10 K.

We conclude that unless a significant number of convective towers can detrain above the tropopause, it is the tropopause cold trap that is the primary dynamical control on stratospheric water vapor. This finding is consistent Ueyama et al. (2015) and with Avery et al. (2017), who noted that about 60% of the El Niño water vapor anomaly could be accounted for by changes in the cold trap temperature alone. We estimate that globally $<$1% of observed SCs penetrate the reanalysis tropopause in Boreal winter, which generally explains the small impact of convection on our computation of stratospheric water.

We can understand the model cloud increase in response to convection in terms of the TTL water vapor budget. Water moves into the TTL primarily through convective injection. Water exits the TTL through ascent into the stratosphere and through gravitational removal as ice. Since there is almost no change in the

stratospheric flux of water when convection is increased, the budget has to be balanced by ice removal, hence the increase in TTLCF.

While the previous studies (S14 and S16) show that, on the average, convection hydrates the UTLS, this is not always the case for individual convective events. For example, if supersaturated air, which is often observed in the TTL (Jensen et al., 2013, 2016; Krämer et al., 2009), encounters a convective system, the in situ vapor will condense on the ice crystals, dehydrating the air. Convective hydration occurs if the air parcel is subsaturated. Thus, there are two types of dehydration events in the TTL: (1) in situ dehydration—due to cloud formation through air parcel cooling and (2) convective dehydration (Jensen et al., 2007). Hydration events occur through convection into subsaturated layers and as a result of ice falling from higher altitude cirrus. We find that convective hydration events exceed dehydration events at all levels in the Boreal winter UTLS. We find that both hydration and dehydration events are mixed together in regions of strong convection as was also noted by Ueyama et al. (2014).

Our results are relevant to understanding the stratospheric HDO distribution. Randel et al. (2012) analysis of HDO data shows a significant Boreal winter asymmetry in HDO depletion around the equator between 15 and 17 km (see their Figure 3). One explanation for the hemispheric asymmetry is that convection is increasing HDO south of the equator by transporting more HDO rich air from the surface to the TTL consistent with the equatorial convective asymmetry shown in Figure 4.

4.2. Convection and Climate

Dessler et al. (2016) found that increased deep convective lofting and ice evaporation can explain the GEOSCCM climate model's increase in stratospheric water above that expected through a secular increase in tropopause temperatures. Our general finding that stratospheric water vapor increases as the convective height increases is in qualitative agreement with the result. But, as noted above, the biggest impact of increasing the convective altitude appears to be the significant increase in TTLCF. SC convection produces significantly more high cloud than MERRA, suggesting that the distribution of convective altitudes is a critical parameter in determining the total cirrus amount. We thus expect the Dessler et al. (2016) GEOS simulation to have produced a large increase in cirrus. That said, most climate models predict a reduction in convective mass flux in a warmer climate (Held & Soden, 2006) with a corresponding decrease in high clouds and a reduction in total cloud feedback (Zelinka & Hartmann, 2011; Zelinka et al., 2012). Our results would also predict a decrease in high clouds if convection is reduced, but a change in the height of convection might also compensate for the reduction in the number of convective cores.

Acknowledgments
Cloud-Aerosol Lidar with Orthogonal Polarization, MLS, MERRA, and MERRA-2 data used in this study are publically available from NASA at no charge. Satellite convection data sets are available through L. Pfister (leonhard.pfister@nasa.gov) at http://bocachica.arc.nasa.gov/~lpfister/cloudtop/. The authors would also like to thank John Kummer and one of the reviewers for useful discussions and insights. This work was supported under NASA grants NNX14AF15G and 80NSSC18K0134.

References

Anderson, J. G., Weisenstein, D., Bowman, K. P., Homeyer, C., Smith, J., Wilmouth, D., et al. (2017). Stratospheric ozone over the United States in summer linked to observations of convection and temperature via chlorine and bromine catalysis. *PNAS*, *114*(25), E4905–E4913.

Anderson, J. G., Wilmouth, D. M., Smith, J. B., & Sayres, D. S. (2012). UV dosage levels in summer: Increased risk of ozone loss from convectively injected water vapor. *Science*, *337*(6096), 835–839. https://doi.org/10.1126/science.1222978

Avery, M. A., Davis, S., Rosenlof, K., Ye, H., & Dessler, A. E. (2017). Large anomalies in lower stratospheric water vapour and ice during the 2015–2016 El Niño. *Nature Geoscience*, *10*(6), 405–409. https://doi.org/10.1038/NGEO2961

Bacmeister, J. T., Eckermann, S. D., Newman, P. A., Lait, L., Chan, K. R., Loewenstein, M., et al. (1996). Stratospheric horizontal wavenumber spectra of winds, temperature, and atmospheric tracers observed by high-altitude aircraft. *Journal of Geophysical Research*, *101*, 9411–9470. https://doi.org/10.1029/95JD03835

Bergman, J. W., Jensen, E. J., Pfister, L., & Yang, Q. (2012). Seasonal differences of vertical-transport efficiency in the tropical tropopause layer: On the interplay between tropical deep convection, large-scale vertical ascent, and horizontal circulations. *Journal of Geophysical Research*, *117*, D05302. https://doi.org/10.1029/2011JD016992,%202012

Bowman, K. P., & Carrie, G. D. (2002). The mean-meridional transport circulation of the troposphere in an idealized GCM. *Journal of the Atmospheric Sciences*, *59*, 1502–1514.

Brewer, A. W. (1949). Evidence for a world circulation provided by the measurements of helium and water vapor distribution in the stratosphere. *Quarterly Journal of the Royal Meteorological Society*, *75*(326), 351–363. https://doi.org/10.1002/qj.49707532603

Corti, T., Luo, B. P., de Reus, M., Brunner, D., Cairo, F., Mahoney, M. J., et al. (2008). Unprecedented evidence for deep convection hydrating the tropical stratosphere. *Geophysical Research Letters*, *35*, L10810. https://doi.org/10.1029/2008GL033641

Danielsen, E. F. (1993). In situ evidence of rapid, vertical, irreversible transport of lower tropospheric air into the lower tropical stratosphere by convective cloud turrets and by larger-scale upwelling in tropical cyclones. *Journal of Geophysical Research*, *98*, 8665–8681. https://doi.org/10.1029/92JD02954

Dessler, A. E., Hanisco, T. F., & Fueglistaler, S. (2007). Effects of convective ice lofting on H_2O and HDO in the tropical tropopause layer. *Journal of Geophysical Research*, *112*, D18309. https://doi.org/10.1029/2007JD008609

Dessler, A. E., Ye, H., Wang, T., Schoeberl, M. R., Oman, L. D., Douglass, A. R., et al. (2016). Transport of ice into the stratosphere and the humidification of the stratosphere over the 21st century. *Geophysical Research Letters*, *43*, 2323–2329. https://doi.org/10.1002/2016GL067991

Frey, W., Borrmann, S., Fierli, F., Weigel, R., Mitev, V., Matthey, R., et al. (2014). Tropical deep convective life cycle: Cb-anvil cloud microphysics from high-altitude aircraft observations. *Atmospheric Chemistry and Physics*, *14*, 13,223–13,240. https://doi.org/10.5194/acp-14-13223-2014

Fueglistaler, S., Dessler, A. E., Dunkerton, T. J., Folkins, I., Fu, Q., & Mote, P. W. (2009). Tropical tropopause layer. *Reviews of Geophysics*, *47*, RG1004. https://doi.org/10.1029/2008RG000267

Gelaro, R., McCarty, W., Suárez, M. J., Todling, R., Molod, A., Takacs, L., et al. (2017). The Modern-Era Retrospective analysis for Research and Applications, version 2 (MERRA-2). *Journal of Climate*, *30*(14), 5419–5454. https://doi.org/10.1175/jcli-d-16-0758.1

Hanisco, T. F., Moyer, E. J., Weinstock, E. M., Clair, J. J. S., Sayres, D. S., Smith, J. B., et al. (2007). Observations of deep convective influence on stratospheric water vapor and its isotopic composition. *Geophysical Research Letters*, *34*, L04814. https://doi.org/10.1029/2006GL027899

Held, I., & Soden, B. (2006). Robust response of the hydrological cycle to global warming. *Journal of Climate*, *19*(21), 5686–5699. https://doi.org/10.1175/JCLI3990.1

Herman, R. L., Ray, E. A., Rosenlof, K. H., Bedka, K. M., Schwartz, M. J., Read, W. G., et al. (2017). Enhanced stratospheric water vapor over the summertime continental United States and the role of overshooting convection. *Atmospheric Chemistry and Physics*, *17*(9), 6113–6124. https://doi.org/10.5194/acp-17-6113-2017

Hertzog, A., & Vial, F. (2001). A study of the dynamics of the equatorial lower stratosphere by use of ultra-long-duration balloons: 2. Gravity waves. *Journal of Geophysical Research*, *106*, 22,745–22,761. https://doi.org/10.1029/2000JD000242

Jensen, E. J., Ackerman, A. S., & Smith, J. A. (2007). Can overshooting convection dehydrate the tropical tropopause layer? *Journal of Geophysical Research*, *112*, D11209. https://doi.org/10.1029/2006JD007943

Jensen, E. J., Diskin, G., Lawson, R. P., Lance, S., Bui, T. P., Hlavka, D., et al. (2013). Ice nucleation and dehydration in the tropical tropopause layer. *PNAS*, *110*(6), 2041–2046. https://doi.org/10.1073/pnas.1217104110

Jensen, E. J., & Pfister, L. (2004). Transport and freeze-drying in the tropical tropopause layer. *Journal of Geophysical Research*, *109*, D02207. https://doi.org/10.1029/2003JD004022

Jensen, E. J., Ueyama, R., Pfister, L., Bui, T., Lawson, P., Woods, S., et al. (2016). On the susceptibility of cold tropical cirrus to ice nuclei abundance. *Journal of the Atmospheric Sciences*, *75*. https://doi.org/10.1175/JAS-D-15-0274.1,%202445-2464

Kärcher, B., Hendricks, J., & Lohmann, U. (2006). Physically based parameterization of cirrus cloud formation for use in global atmospheric models. *Journal of Geophysical Research*, *111*, D01205. https://doi.org/10.1029/2005JD006219

Keith, D. (2000). Stratosphere-troposphere exchange: Inferences from the isotopic composition of water vapor. *Journal of Geophysical Research*, *105*, 15,167–15,173. https://doi.org/10.1029/2000JD900130

Khaykin, S., Pommereau, J.-P., Korshunov, L., Yushkov, V., Nielsen, J., Larsen, N., et al. (2009). Hydration of the lower stratosphere by ice crystal geysers over land convective systems. *Atmospheric Chemistry and Physics*, *9*, 2275–2287.

Kim, J.-E., & Alexander, M. J. (2013). A new wave scheme for trajectory simulations of stratospheric water vapor. *Geophysical Research Letters*, *40*, 5286–5290. https://doi.org/10.1002/grl.50963

Kley, D., Schmeltekopf, A. L., Kelly, K., Winkler, R. H., Thompson, T. L., & McFarland, M. (1982). Transport of water through the tropical tropopause. *Geophysical Research Letters*, *9*, 617–620. https://doi.org/10.1029/GL009i006p00617

Krämer, M., Schiller, C., Afchine, A., Bauer, R., Gensch, I., Mangold, A., et al. (2009). Ice super-saturations and cirrus cloud crystal numbers. *Atmospheric Chemistry and Physics*, *9*(11), 3505–3522. https://doi.org/10.5194/acp-9-3505-2009

Livesey, N., Read, W. G., Wagner, P. A., Froidevaux, L., Lambert, A., Manney, G. L., et al. (2017). Aura Microwave Limb Sounder (MLS) version 4.2x level 2 data quality and description document, JPL D-33509 Rev. C.

Molod, A., Takacs, L., Suarez, M., & Bacmeister, J. (2015). Development of the GEOS-5 atmospheric general circulation model: Evolution from MERRA to MERRA-2. *Geoscientific Model Development*, *8*(5), 1339–1356. https://doi.org/10.5194/gmd-8-1339-2015

Moorthi, S., & Suarez, M. J. (1992). Relaxed Arakawa-Schubert, a parameterization of moist convection for general-circulation models. *Monthly Weather Review*, *120*(6), 978–1002. https://doi.org/10.1175/1520-0493(1992)120%3C0978:RASAPO%3E2.0.CO;2

Moyer, E., Irion, F., Yung, Y., & Gunson, M. (1996). ATMOS stratospheric deuterated water and implications for troposphere-stratosphere transport. *Geophysical Research Letters*, *23*, 2385–2388. https://doi.org/10.1029/96GL01489

Podglajen, A., Hertzog, A., Plougonven, R., & Legras, B. (2016). Lagrangian temperature and vertical velocity fluctuations due to gravity waves in the lower stratosphere. *Geophysical Research Letters*, *43*, 3543–3553. https://doi.org/10.1002/2016GL068148

Pollock, W., Heidt, L. E., Lueb, R., & Ehhalt, D. H. (1980). Measurement of stratospheric water vapor by cryogenic collection. *Journal of Geophysical Research*, *85*, 5555–5568. https://doi.org/10.1029/JC085iC10p05555

Randel, W. J., & Jensen, E. J. (2013). Physical processes in the tropical tropopause layer and their roles in changing climate. *Nature Geoscience*, *6*(3), 169–176. https://doi.org/10.1038/NGEO1733

Randel, W. J., Moyer, E., Park, M., Jensen, E., Bernath, P., Walker, K., & Boone, C. (2012). Global variations of HDO and HDO/H2O ratios in the UTLS derived from ACE-FTS satellite measurements. *Journal of Geophysical Research*, *117*, D06303. https://doi.org/10.1029/2011JD016632

Randel, W. J., & Wu, F. (2005). Kelvin wave variability near the equatorial tropopause observed in GPS radio occultation measurements. *Journal of Geophysical Research*, *110*, D03102. https://doi.org/10.1029/2004JD005006

Sayres, D. S., Pfister, L., Hanisco, T. F., Moyer, E. J., Smith, J. B., Clair, J. M. S., et al. (2010). Influence of convection on the water isotopic composition of the tropical tropopause layer and tropical stratosphere. *Journal of Geophysical Research*, *115*, D00J20. https://doi.org/10.1029/2009JD013100

Schoeberl, M., Dessler, A., Ye, H., Wang, T., Avery, M., & Jensen, E. J. (2016). The impact of gravity waves and cloud nucleation threshold on stratospheric water and tropical tropospheric cloud fraction. *Earth and Space Science*, *3*, 295–305. https://doi.org/10.1002/2016EA000180

Schoeberl, M. R., & Dessler, A. E. (2011). Dehydration of the stratosphere. *Atmospheric Chemistry and Physics*, *11*(16), 8433–8446. https://doi.org/10.5194/ASC-11-8433-2011,%208433-8446

Schoeberl, M. R., Dessler, A. E., Wang, T., Avery, M. A., & Jensen, E. J. (2014). Cloud formation, convection, and stratospheric dehydration. *Earth and Space Science*, *1*, 1–17. https://doi.org/10.1002/2014EA000014

Schoeberl, M. R., Jensen, E., Podglajen, A., Coy, L., Lodha, C., Candido, S., & Carver, R. (2017). Gravity wave spectra in the lower stratosphere diagnosed from Project Loon balloon trajectories. *Journal of Geophysical Research Atmospheres*, *122*, 8517–8524. https://doi.org/10.1002/2017JD026471

Schoeberl, M. R., Jensen, E. J., & Woods, S. (2015). Gravity waves amplify upper tropospheric dehydration by clouds. *Earth and Space Science*, *2*, 485–500. https://doi.org/10.1002/2015EA000127

Schwartz, M. J., Read, W. G., Santee, M. L., Livesey, N. J., Froidevaux, L., Lambert, A., & Manney, G. L. (2013). Convectively injected water vapor in the North American summer lowermost stratosphere. *Geophysical Research Letters*, *40*, 2316–2321. https://doi.org/10.1002/grl.50421

Sherwood, S. C., & Risi, C. (2012). The HDO/H2O relationship in tropospheric water vapor in an idealized "last-saturation" model. *Journal of Geophysical Research*, *117*, D19205. https://doi.org/10.1029/2012JD018068

Smith, J. B., Wilmouth, D. M., Bedka, K. M., Bowman, K. P., Homeyer, C. R., Dykema, J. A., et al. (2017). A case study of convectively sourced water vapor observed in the overworld stratosphere over the United States. *Journal of Geophysical Research: Atmospheres*, *122*, 9529–9554. https://doi.org/10.1002/2017JD026831

Son, S.-W., & Lee, S. (2007). Intraseasonal variability of the zonal-mean tropical tropopause height. *Journal of the Atmospheric Sciences*, *64*(7), 2695–2706. https://doi.org/10.1175/JAS3982A.1

Sun, Y., & Huang, Y. (2015). An examination of convective moistening of the lower stratosphere using satellite data. *Earth and Space Science*, *2*, 320–330. https://doi.org/10.1002/2015EA000115

Thuburn, J., & Craig, G. (2002). On the temperature structure of the tropical substratosphere. *Journal of Geophysical Research*, *107*, 4017. https://doi.org/10.1029/2001JD000448

Ueyama, R., Jensen, E. J., Pfister, L., Diskin, G. S., Bui, T. P., & Dean-Day, J. M. (2014). Dehydration in the tropical tropopause layer: A case study for model evaluation using aircraft observations. *Journal of Geophysical Research: Atmospheres*, *119*, 5299–5316. https://doi.org/10.1002/2013JD021381

Ueyama, R., Jensen, E. J., Pfister, L., & Kim, J.-E. (2015). Dynamical, convective, and microphysical control on wintertime distributions of water vapor and clouds in the tropical tropopause layer. *Journal of Geophysical Research: Atmospheres*, *120*, 10,483–10,500. https://doi.org/10.1002/2015JD023318

Ye, H., Dessler, A. E., & Yu, W. (2017). Effects of tropical deep convection on interannual variability of tropical tropopause layer water vapor. *Atmospheric Chemistry and Physics Discussions*. https://doi.org/10.5194/acp-2017%E2%80%93951

Zelinka, M. D., & Hartmann, D. L. (2011). The observed sensitivity of high clouds to mean surface temperature anomalies in the tropics. *Journal of Geophysical Research*, *116*, D23103. https://doi.org/10.1029/2011JD016459

Zelinka, M. D., Klein, S. A., & Hartmann, D. L. (2012). Computing and partitioning cloud feedbacks using cloud property histograms. Part II attribution to changes in cloud amount, altitude, and optical depth. *Journal of Climate*, *25*, 3736–3754.

Zhou, X., & Holton, J. R. (2002). Intraseasonal variations of tropical cold-point tropopause temperatures. *Journal of Climate*, *15*(12), 1460–1473. https://doi.org/10.1175/1520-0442(2002)015%3C1460:IVOTCP%3E2.0.CO;2